Geomorphology 457 (2024) 109228

Contents lists available at ScienceDirect

Geomorphology

journal homepage: www.journals.elsevier.com/geomorphology

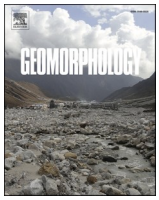

Digital topographic analysis and lineament interpretation south of the Lena Delta, North Siberia: Landscape expression of its tectonic activity

Jakob S. Hamann [a,b,*], Alisa V. Baranskaya [c], Wolfram H. Geissler [a], Boris V. Baranov [d], Nikolay V. Tsukanov [d]

[a] Alfred Wegener Institute, Helmholtz Centre for Polar and Marine Research, Bremerhaven 27570, Germany
[b] Department of Earth Sciences, Physical Geography, Freie Universität Berlin, Berlin 12249, Germany
[c] Faculty of Geography, Lomonosov Moscow State University, Moscow, Russia
[d] Shirshov Institute of Oceanology, Russian Academy of Sciences, Moscow, Russia

ARTICLE INFO

Keywords:
Tectonic Geomorphology
Lineament Identification
Topographic Analysis
Hypsometry
Arctic Landscapes

ABSTRACT

This study applies semi-automated techniques to analyze the landforms, morphostructure, and geology of the Kharaulakh and Chekanovsky sectors, south of the Lena Delta, northern Siberia. High-resolution data, including TanDEM-X 30 m spatial resolution Digital Elevation Models (DEM), 2 m spatial resolution ArcticDEM Digital Surface Models (DSM), and Sentinel-2 satellite imagery, serve as the basis for the analysis. Digital terrain classification and identification of tectonic lineaments are performed using the Benthic Terrain Modeler (BTM) and Linear Extraction (LINE) algorithm, respectively. Additionally, a hypsometric analysis is conducted to assess areas of potential neotectonic activity. 873 lineaments are identified, primarily in NE-SW and E-W orientations. NW-SE lineaments perpendicular to the lithological and fold belt strikes in the Kharaulakh Ridge suggest inheritance from original depositional settings or later compressional tectonics, now appearing as valleys and weak zones facilitating erosion and river incision. Longer N-S or NNW-SSE lineaments in the Kharaulakh Sector are associated with thrust sheets of the Verkhoyansk fold-and-thrust belt and Cenozoic graben structures linked to the formation of the Laptev Sea Rift System and ongoing regional deformation. The Chekanovsky Sector, marked by epiplatform blocks and hills, presents a dissected plateau with steep valleys. Here, high hypsometric integral values are attributed to compression and uplift near the southwestern boundary of the Laptev Sea Microplate.

1. Introduction

Geomorphological studies utilizing automated classification techniques with Digital Elevation Models (DEM) and satellite imagery, integrated into geographical information systems (GIS) or remote sensing software, have significantly advanced our understanding of topographic evolution in recent years (e.g., Drăguţ and Blaschke, 2006; Piloyan and Konečný, 2017; Gioia et al., 2021). These methods provide a more efficient and objective approach, supplementing traditional geomorphological methods reliant on extensive fieldwork, manual processing of topographic maps, and interpretation of aerial photographs. A comprehensive geomorphological analysis is essential for comprehending landscape evolution, covering erosional, depositional, and tectonic processes (Huggett and Shuttleworth, 2022). This study focuses on lineaments, which are linear features in a landscape indicating underlying geological displacement zones, such as faults or fractures (O'Leary et al., 1976). Major faults often exhibit a topographic expression due to surface displacement, differential erosion of juxtaposed rock units, and erosion of damaged rocks (Henderson et al., 1996). Mature fault zones typically consist of a central fault core and a surrounding damage zone (e.g., Vermilye and Scholz, 1998; Faulkner et al., 2011; Brandes and Tanner, 2020), which are susceptible to erosion due to their weak material (e.g., Roy et al., 2016; Upton et al., 2018). Remote sensing technologies, such as aerial photographs, satellite imagery, and DEMs, thus allow to identify faults and have been utilized in many lineament analysis studies (e.g., Jordan and Schott, 2005; Scheiber et al., 2015; Ahmadi and Pekkan, 2021). Recent advances in image processing and pattern recognition through improved computer hardware and spatial-analysis methods have made automatic lineament extraction techniques possible (e.g., Masoud and Koike, 2011; Bonetto et al., 2015; Assatse et al., 2016; Elmahdy et al., 2019).

This study aims to conduct terrain and lineament analyses utilizing

* Corresponding author at: Alfred Wegener Institute, Helmholtz Centre for Polar and Marine Research, Bremerhaven 27570, Germany.
E-mail address: jakob.hamann467@gmail.com (J.S. Hamann).

https://doi.org/10.1016/j.geomorph.2024.109228
Received 25 October 2023; Received in revised form 22 April 2024; Accepted 23 April 2024
Available online 27 April 2024

DEMs and Sentinel-2 satellite images with automated detection tools in GIS and remote sensing software for an area with Mesozoic, Cenozoic, and recent tectonic activity along the SW coastal region of the Laptev Sea, northern Siberia to reveal the main landscape expressions of its tectonic setting. Additionally, a hypsometric analysis is employed to infer potential neotectonic activity and interpret the dominant landscape-shaping processes and dynamics. The hypsometric analysis provides a valuable means of identifying and quantifying relationships between the topography, tectonic activity, and surface processes (e.g., Siddiqui and Soldati, 2014; Farhan et al., 2016; Andreani et al., 2014; Buczek and Górnik, 2020).

The study area includes the Kharaulakh and Chekanovsky sectors (Fig. 1), influenced by continental rifting in the Laptev Sea, and continental compressional tectonics of the Verkhoyansk fold-and-thrust belt. While previous studies in the Kharaulakh Sector have primarily focused on seismology, structural geology, and tectonics (e.g., Fujita et al., 2009; Imaeva et al., 2016, 2017, 2019; Imaev et al., 2018), there has been limited studies in the field of digital topography and lineament analyses of local structures (Grosse et al., 2007; Baranskaya, 2013; Parfenov and Kuzmin, 2001). The analysis of landforms and hypsometry offers insights into the dynamics of landscapes at a regional scale, highlighting primary exogenic and endogenic processes. Digital lineament analysis using GIS can offer an overview of potential tectonic features, which can be further validated through future geological and geophysical surveys for better understanding of the area's tectonic evolution in the past and present.

2. Geological and geomorphological structure of the Kharaulakh and Chekanovsky sectors

The Kharaulakh and Chekanovsky sectors, located along the Laptev Sea coastal region of the northern Siberian mainland, are strongly influenced by the region's continental climate, periglacial processes, and tectonics (Grosse et al., 2007; Schirrmeister et al., 2022; Parfenov et al., 1995; Imaev et al., 2018). The Kharaulakh Sector comprises two main geological domains: the uplifted Kharaulakh Ridge and the subsiding coastal regions, including the Bykovsky Peninsula (Grosse et al., 2007). During the Last Glacial Maximum (LGM), around 26,000 to 19,000 years ago, when sea level was approximately 120 m lower than today (Fairbanks, 1989), the Bykovsky Peninsula formed part of a wider depositional plain (Grosse et al., 2007). The northern Verkhoyansk Range, due to its strong continental climate, was not covered by any ice sheets during the LGM (Hubberten et al., 2004; Svendsen et al., 2004; Stauch and Lehmkuhl, 2010). Consequently, periglacial, fluvial, and tectonic processes played a crucial role in the Holocene landscape evolution.

The Kharaulakh Sector is part of the Verkhoyansk fold-and-thrust belt, which itself belongs to a large Mesozoic to Cenozoic orogenic belt, spanning approximately 2000 km in length and 500 km in width (Parfenov et al., 1995). It is located along the eastern margin of the Siberian platform and is the largest fold-and-thrust belt on Earth. The Chekanovsky Sector is not associated with the Verkhoyansk complex and forms part of the stable Siberian Craton. The Kharaulakh and Chekanovsky sectors comprise several NE-SW orientated linear structures which were interpreted earlier as fractures of Mesozoic folding stages

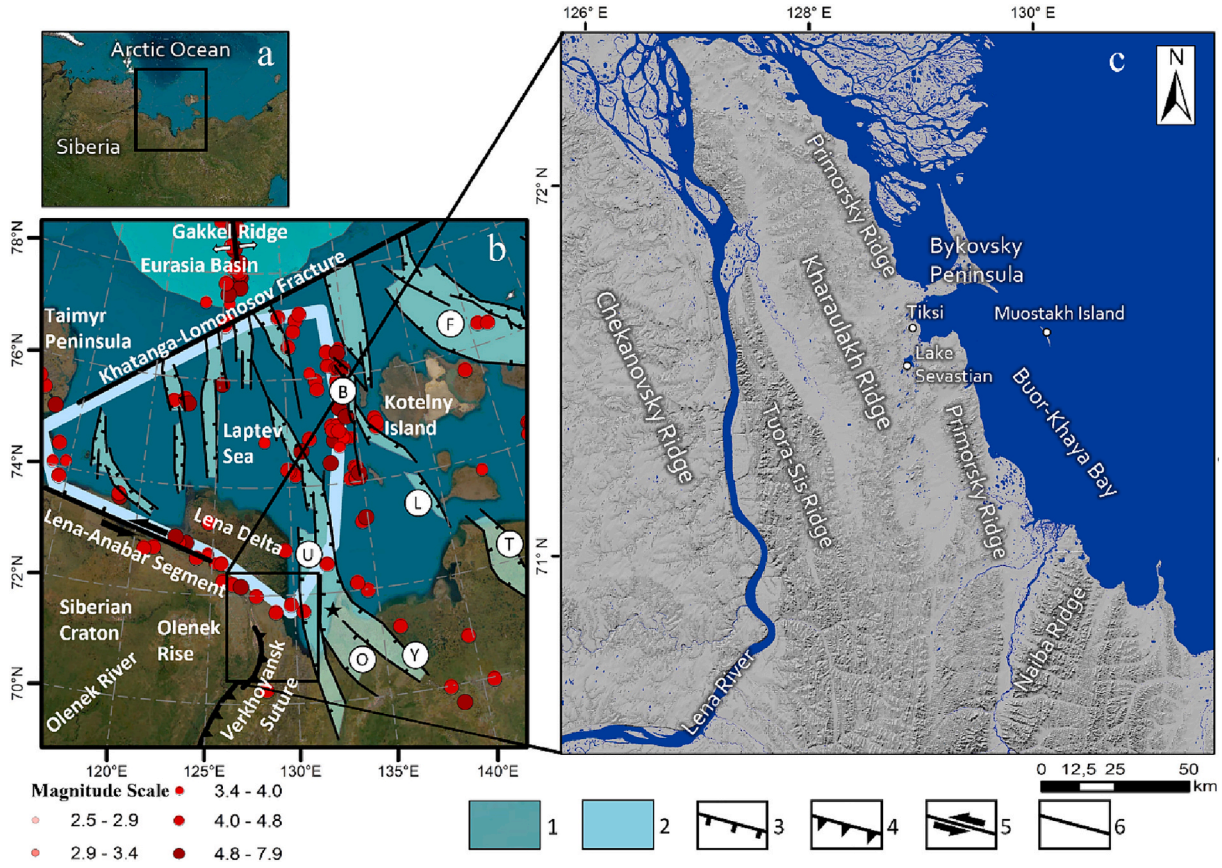

Fig. 1. Study area. (a) Location of the study area in northern Siberia (black box). (b) Study area including regional Cenozoic tectonic features, modified after Imaeva et al. (2016). (1) Rift troughs (letters in circles): Faddeyevsky (F), Belkovsky-Svyatonsky (B), Lyakhovsky (L), Ust'-Lena (U), Tastakh (T), Ust-Yana' (Y), Omoloi (O); (2) Laptev Sea Microplate boundary; (3) normal faults; (4) reverse faults and overthrusts; (5) strike-slip faults; (6) transform faults. The asterisk indicates the rotation pole of the Eurasian and North American plates (Imaeva and Kolodeznikova, 2017). The red dots represent all recorded earthquakes with a magnitude >2.5 from 1973 to 2018 (sourced: U.S. Geological Service). (c) Hillshade map of the Kharaulakh and Chekanovsky sectors. (For interpretation of the references to color in this figure legend, the reader is referred to the web version of this article.)

(Imaeva et al., 2016, 2017). Ongoing erosion and fluvial processes resulted in the formation of numerous valleys, with the Khorogor Valley being the largest, influenced by two major striking faults along its boundaries (Grosse et al., 2007). The Kharaulakh Sector also contains broad depressions from Paleogene rifting phases (Imaeva et al., 2016) and smaller depressions mainly due to thermokarst (Grosse et al., 2007).

The Kharaulakh and Chekanovsky sectors are part of a complex transition zone influenced by the Gakkel Ridge's oceanic spreading to the north, ongoing continental rifting in the adjacent Laptev Sea, and potential compressional/transpressional tectonics to the south/southeast (Avetisov, 2000; Grachev et al., 1970; Fujita et al., 2009; Imaev et al., 2018; Imaeva et al., 2020). Seismicity and deformation concentrate along the mid-ocean ridge in the north and are widely spread across the Laptev Sea Shelf's horsts and grabens (Fig. 1) forming the Laptev Sea Microplate (LSM). The eastern LSM boundary corresponds to a seismically active zone extending from the Gakkel spreading ridge to the Buor-Khaya Bay and further south to the Kharaulakh Ridge. Earthquakes along this boundary zone display extensional or transtensional focal mechanisms with fault planes parallel to the grabens on the Laptev Sea Shelf (Avetisov, 2000; Imaev et al., 2018; Imaeva et al., 2020).

In the Kharaulakh Sector, the geodynamics significantly change due to its location at a triple junction near the rotation pole of the Eurasian and North American plates (Fig. 1). The crust's stress state varies, leading to normal faulting, strike-slip faulting, thrust faulting, and combinations (Imaev et al., 2018). The southwestern boundary of the LSM, spanning along the Laptev Sea's southwestern coast from the Taimyr Peninsula to the Buor-Khaya Bay (Fig. 1), corresponds to a zone of increased seismic activity related to the Lena-Taimyr uplifts (Avetisov, 2000).

The sedimentary sequences in both studied sectors range from the late Proterozoic to recent times (Imaev et al., 2018), with the Kharaulakh Sector being dominated by Permian sandstones, siltstones, and mudstones overlying a sequence of Carboniferous sedimentary rocks (Imaeva et al., 2019). In contrast, the Chekanovsky Sector consists mainly of Mesozoic sandstones (Bidzhiev, 1970; Gogina et al., 1971).

3. Data

This study employs Sentinel-2 satellite imagery, high-resolution ArcticDEM (2 m), and 30 m TanDEM-X DEM for geomorphological, lineament, and hypsometric analysis in the Kharaulakh and Chekanovsky sectors.

Sentinel-2 is a satellite imaging mission developed by the European Space Agency (ESA) as part of the Copernicus Earth Observation Program (Drusch et al., 2012). It offers spatial resolutions ranging from 10 m to 60 m and 13 spectral bands, surpassing missions like Landsat.

ArcticDEM (Porter et al., 2018), an initiative by the National Science Foundation and the Geospatial-Intelligence Agency, compiles high-resolution Digital Surface Models (DSM) capturing surface features, including natural and artificial structures like vegetation and buildings.

TanDEM-X is an Earth observation satellite by the German Aerospace Center and Aerospace manufacturer EADS Astrium (now Airbus Defence and Space), compiling DEMs of Earth's land surface up to 12 m resolution (Zink et al., 2014). This study utilizes the 30 m TanDEM-X variant, which offers smoother geoprocessing compared to the 12 m version.

4. Methods

4.1. Geomorphology

The geomorphological classification integrates interpretations from satellite imagery, DEMs, geological data, and the results of a semi-automatic terrain classification by the Benthic Terrain Modeler (BTM), complemented by field observations.

The BTM is an ArcGIS extension used to classify benthic terrain into geomorphological classes (Lundblad et al., 2006; Wright et al., 2012; Walbridge et al., 2018). It was developed by the National Oceanic and Atmospheric Administrations (NOAA) Coastal Services Center and the Environmental System Research Institute (ESRI).

The BTM integrates geoprocessing spatial analysis tools to combine terrain parameters and produce a classified topographic map using digital elevation data as basis (Fig. 2). The core component of the BTM is the Bathymetric Position Index (BPI), which is a modification of the Topographic Position Index (TPI) by Weiss (2001). The TPI has found widespread use in the field of geomorphology (e.g., De Reu et al., 2013; Mokarram et al., 2015; Skentos, 2017; Muddarisna et al., 2020) since the creation of an ArcGIS extension by Jenness (2006). The BPI, like the TPI, measures the relative elevation of each pixel or grid cell in an elevation model compared to the average elevation of surrounding pixels within a specified neighborhood. This helps to identify topographic and bathymetric features by highlighting areas that are significantly higher, lower, or at a similar level to their surroundings. One advantage of the BPI is its differentiation into Broad Scale BPI and Fine Scale BPI, which concentrate on larger and smaller neighborhoods, respectively, to integrate features of different scale. Hence, the BTM algorithm is used for this study.

The outputs for slope and the broad- and fine-scale standardized BPI's are defined together with the DEM through a classification dictionary, which classifies these numerical values into categories of terrain (Fig. 2). The Classification Dictionary assigns specific terrain features, such as valleys, ridges, flat plains, or slopes, based on predefined ranges of slope and BPI values. The result is a classified terrain raster where each pixel or grid cell is labeled with its terrain category.

Two separate BTM analyses are performed in this study. The first analysis (referred to as M1) covers the entire research area, while the second analysis (M2) focuses on the central Kharaulakh Sector. M1 is composed of 22 TanDEM-X 30 m DEMs and M2 of four ArcticDEM DSMs, respectively. The input parameters for the BPI analysis differ between M1 and M2 due to differences in spatial resolution and scale. For M1, the broad-scale analysis is conducted with inner and outer radii of 3 and 10 pixels, respectively, and 1 and 3 pixels for the fine scale analysis. For M2, inner and outer radii of 100 and 1000 pixels, respectively, are employed for broad-scale analysis, with 10 and 100 pixels used for the fine-scale analysis. The Classification Dictionary is modified after Erdey-Heydorn (2008) and Goes et al. (2019). Mountain tops and outcrops are defined by positive BPI values greater than one standard deviation (−1/+1 standard deviation corresponds to 100/+100 in Classification Dictionary) from the mean. Valleys and depressions are defined by areas with negative BPI values greater than one standard deviation from the mean in the negative direction. The degree of slope defines flat areas, gentle slopes, and steep slopes (Table 1).

Water bodies and flat plains are merged due to their intermixing in low-lying coastal regions (Suppl. Fig. S1). Hence, to accurately represent water bodies, the high-resolution World Ocean Basemap of ArcGIS 10. 8 is used as a reference grid. Furthermore, the elevation values in the ArcticDEM DSMs are corrected. A comparison between the elevation values of ArcticDEM DSMs and those from TanDEM-X 30 m DEMs and satellite imagery reveals that the ArcticDEM DSMs register elevation values 8 m (±1 m) lower than the actual elevation. This inaccurately portrays features like the Bykovsky Peninsula as partially submerged. Therefore, the ArcticDEM DSMs are adjusted by +8 m using ArcGIS's Raster Calculator.

Landforms are then categorized manually based on their structural, tectonic, accumulative, or erosive characteristics, alongside their spatial context and morphological features identified in satellite imagery, geological data, field data, DEMs, and the results of the BTM terrain classification (Fig. 3). BTM-identified valleys of M1 add a distinct class defined solely by morphology. Additionally, flat plains defined by the BTM serve to delineate clear boundaries, distinguishing flat graben bottoms from other landforms. Gentle slopes are identified by the BTM algorithm; however, they are portrayed only where they visibly represent sloped erosive and accumulative features (alluvial fans, pediment)

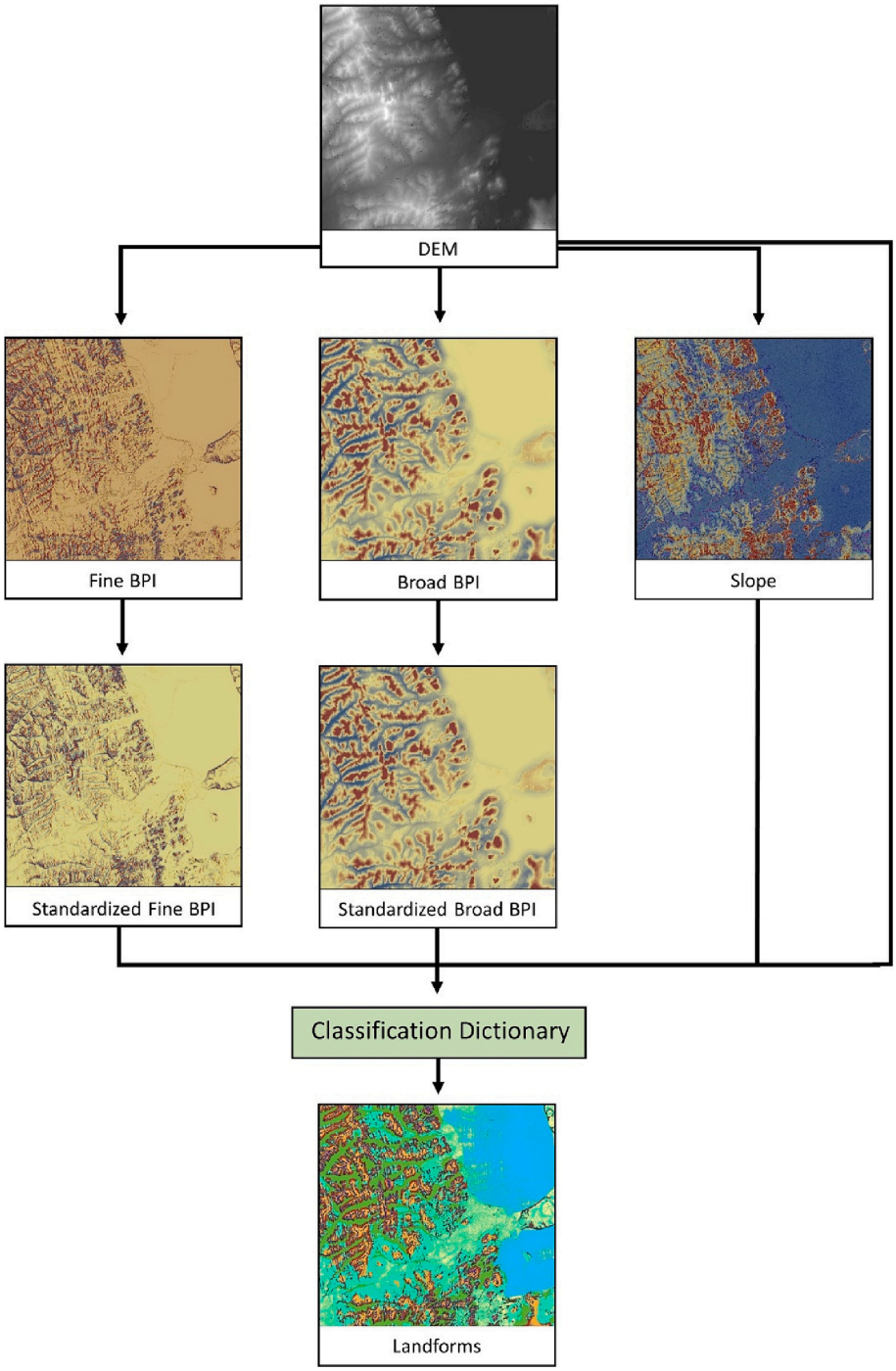

Fig. 2. Workflow of the BTM. A series of geoprocessing spatial analyses classifies the landscape into defined terrain categories.

Table 1
Classification Dictionary for the terrain classification of the BTM, modified after Erdey-Heydorn (2008) and Goes et al. (2019).

Classification		Broad Scale BPI		Fine Scale BPI		Slope		Elevation	
Class	Structures	Lower	Upper	Lower	Upper	Lower	Upper	Lower	Upper
1	Flat Plains	−100	100	−100	100		1	0	
2	Depression	−100	100		−100				
3	Gentle Slopes	−100	100	−100	100	1	5		
4	Steep Slopes	−100	100	−100	100	5			
5	Flat Ridge Tops	100		−100	100				
6	Rock Outcrop Highs	100		100	100				
7	Valleys		−100						
8	Water	−100	100	−100	100			−10	0

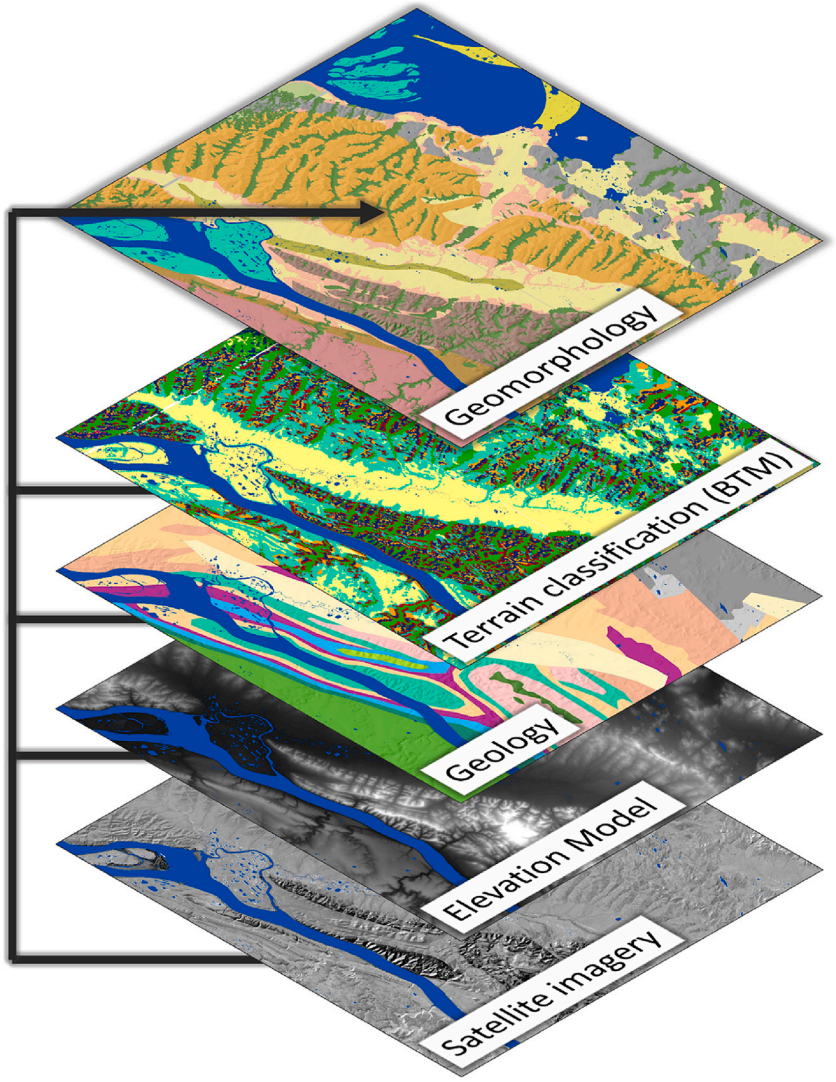

Fig. 3. Workflow of the geomorphological classification. The arrow represents the comparison and mutual validation of all data sources.

of adjacent structural landscapes.

Fieldwork in the areas of Tiksi, Lake Sevastian, and Muostakh Island (see Fig. 1) was conducted in 2011 as part of the Lena-2011 expedition. The field studies involved geomorphological description of landscapes, geomorphological profiling, and observations of geological composition, faults, and jointing. The collected data were utilized for the classification of landforms in the Kharaulakh Sector. Additionally, photographs were taken in the years 2015 to 2019 to document the landscape surrounding potential and actual sites for the deployment of temporary seismological stations along the Lena River, in the Lena Delta and along the Buor Khaya coast. These photographs contributed to the topographic analysis of both the Kharaulakh and Chekanovsky sectors.

4.2. Lineaments

The LINE (Linear Extraction) algorithm in PCI Geomatics software is utilized to semi-automatically delineate linear features from Sentinel-2 satellite imagery. LINE consists of three steps: edge detection, thresholding, and curve extraction. It utilizes the Canny Edge Detection algorithm for edge detection, followed by thresholding and curve extraction to generate vector segments representing the linear features. To supervise the lineament extraction, the LINE algorithm requires six input-parameters: Filter Radius (RADI), Edge Gradient Threshold (GTHR), Curve Length Threshold (LTHR), Line Fitting Error Threshold (FTHR), Angular Difference Threshold (ATHR), and Linking Distance Threshold (DTHR). The final polylines are saved as vector segments for further use in ArcGIS.

Table 2
LINE parameters and respective values in pixels, meters, and degrees utilizing Sentinel-2 imagery (band-8).

Abbreviation	Caption	Default value	Chosen value	Corresponding value in meters (or degrees)
RADI	Filter Radius	10	10	100 m
GTHR	Edge Gradient Threshold	100	50	500 m
LTHR	Curve Length Threshold	30	30	300 m
FTHR	Line Fitting Error Threshold	3	3	30 m
ATHR	Angular Difference Threshold	30	15	15°
DTHR	Linking Distance Threshold	20	20	200 m

Sentinel-2 satellite imagery's band-8 (near-infrared) with a spatial resolution of 10 m is utilized for the LINE analysis, as Javhar et al. (2019) identified it as the most effective band for automatic lineament extraction techniques. The input parameters (Table 2) are selected to achieve a balance between line segment density and length.

A second analysis employs eleven ArcticDEM DSMs as input imagery. The parameters for this analysis are adjusted to accommodate the high spatial resolution of ArcticDEM DSMs, resulting in modified values (Table 3).

After the LINE algorithm is applied to Sentinel-2 satellite imagery and ArcticDEM DSMs, the outcomes are analyzed together with visual interpretations of Sentinel-2 satellite imagery, TanDEM-X 30 m DEMs, previous geological studies, and a hydrology network analysis. Rose diagrams of the mapped lineaments are generated using Rock-Works17 software (RockWare, n.d.).

Topographic features like linear valleys, systematic offsets of rivers, straight rock boundaries, or continuous scarps are often indicative of underlying geological structures and are thus interpreted as lineaments. Sentinel-2 satellite imagery is particularly useful for visual interpretation, as it provides the best exposure to differences in sedimentary bedding. TanDEM-X 30 m DEMs provide elevation data that expose morphological structures like valleys. The calibration of a hydrology network for the study area is performed through an ArcGIS hydrology spatial analysis based on TanDEM-X 30 m DEMs (Suppl. Fig. S2). Linear flow-paths can illustrate drainage patterns influenced by tectonic processes (e.g., Mallast et al., 2011; Psomiadis et al., 2020). This study's lineament interpretations are also cross-referenced with geological maps of the study area (Bidzhiev, 1970; Gogina et al., 1971; Bijiyev and Gorshkova, 1975; Gogina, 1975; Andreev et al., 1981).

4.3. Hypsometry

Hypsometry analyzes the elevation distribution within a study area and is quantified through the hypsometric integral (HI) and hypsometric curve (Strahler, 1952; Schumm, 1956). HI values are dimensionless, range from 0 to 1 and serve as indicators to describe the evolution of watersheds (e.g., Strahler, 1952; Ohmori, 1993; Willgoose and Hancock, 1998; Pérez-Peña et al., 2009; Duan et al., 2022). The HI is defined as the area below the hypsometric curve and can be calculated using the following equation:

$$\mathrm{HI} = (\text{mean elevation} - \textit{min}\ \text{elevation})/(\textit{max}\ \text{elevation} - \textit{min}\ \text{elevation}) \quad (1)$$

High HI values (HI >0.5) are indicative of young landscapes, suggesting areas of recent uplift, characterized by high erosion potential and significant relief with more pronounced geological formations (e.g., Siddiqui and Soldati, 2014; Farhan et al., 2016; Andreani et al., 2014). Conversely, low values (HI <0.3) are considered to represent more mature landscapes, indicative of tectonic stability or advanced erosion stages, with smoother terrains and few sharp topographical features (e.g., El Hamdouni et al., 2008; Mahmood and Gloaguen, 2012). However, low values can also be attributed to young depositional plains or other flat landscapes (e.g., Andreani et al., 2014).

For the hypsometric analysis, the study area is divided into terrain segments to assess the geomorphic state of topographically distinct regions by calculating their respective HI values. This involves a series of hydrological analyses in ArcGIS utilizing TanDEM-X 30 m DEMs (Fig. 4). The hydrology network from the lineament classification serves as basis. Pour points are manually placed primarily at the bases of catchments or stream flows to widen uphill structural forms rather than lower-elevation depositional landforms. Subsequently, the *Watershed* function is applied using the flow direction raster and pour points. The terrain segments are then merged based on similar catchment areas, topography, and drainage dynamics, reducing their number from 213 to 105 for the study area. Each terrain segment is extracted as a DEM using the ArcGIS *Extract by Mask* function. The HI values are subsequently calculated, and hypsometric curves are visualized for each DEM using R software (R Core Team, 2021).

5. Results

5.1. Geomorphology

The BTM terrain classification for M1 (Fig. 5) identifies water as the dominant category, covering 27.3 % of the study area, followed by flat plains (23.8 %) and gentle slopes (17.6 %). Valleys (7.9 %), rock outcrops (4.2 %), flat ridge tops (3.4 %), steep slopes (3.6 %) and depressions (2.6 %) make up the rest of terrain categories. Notably, 9.6 % of the area is classified as 'no data'; however, these areas are exclusively located over water bodies, thus not affecting the terrain analysis.

For M2 (Fig. 6), gentle slopes are the most dominant class, accounting for 28.1 % of the study area, followed by flat plains (20.9 %) and water (18.6 %). Percentages for valleys (9.9 %), flat ridge tops (5.5 %), rock outcrops (3.6 %), and depressions (2.5 %) are similar to those in M1. However, M2 has a greater proportion of steep slopes (8.3 %), which is attributed to the higher resolution of the analysis. Like M1, 'no data' areas in M2 (2.6 %) are over water.

The geomorphological analysis (Fig. 7) reveals landscapes of structural origin, where topography reflects geological structures, and landscapes of tectonic origin shaped by movements of the Earth's crust, alongside accumulative topography. Within the Chekanovsky Sector, epiplatform block mountains and hills of the Siberian Craton (class 1 and 2, Fig. 7) dominate, characterized by low mountains with elevations up to 500 m. The contact zone between the Siberian Craton and the Verkhoyansk fold-and-thrust belt is evident on both coasts of the Lena River valley, expressed as gentle slopes descending towards the river (class 3, Fig. 7). Most of the Kharaulakh Sector lies within the Verkhoyansk fold-and-thrust belt. The highest part, the Tuora-Sis Ridge with mountains reaching elevations up to 900 m (class 4 in Fig. 7), comprises fold and block mountains and ridges, where the topography reflects folding, alongside blocks displaced along younger faults. Further east, closer to the Buor-Khaya Bay, low (400–500 m) fold and residual mountains are located (classes 4, 5, and 6, Fig. 7), characterized by shapes and structures mainly inherited from folds formed during the folding of the Verkhoyansk system. These mountains flank the Naiba Rift (classified separately as class 7 and eastern part of class 6 in Fig. 7) as their topography has evolved under the influence of the rift-related uplift. All these mountains are dissected by grabens and rifts. While the bottoms of such grabens are flat (classes 8 and 9, Fig. 7), they have a rocky basement and are rarely covered by Quaternary sediments. Accumulative

Table 3
LINE parameters and respective values in pixels, meters, and degrees utilizing ArcticDEM DSMs.

Abbreviation	Caption	Default value	Chosen value	Corresponding value in meters (or degrees)
RADI	Filter Radius	10	10	100 m
GTHR	Edge Gradient Threshold	100	200	400 m
LTHR	Curve Length Threshold	30	100	200 m
FTHR	Line Fitting Error Threshold	3	20	40 m
ATHR	Angular Difference Threshold	30	60	60°
DTHR	Linking Distance Threshold	20	50	100 m

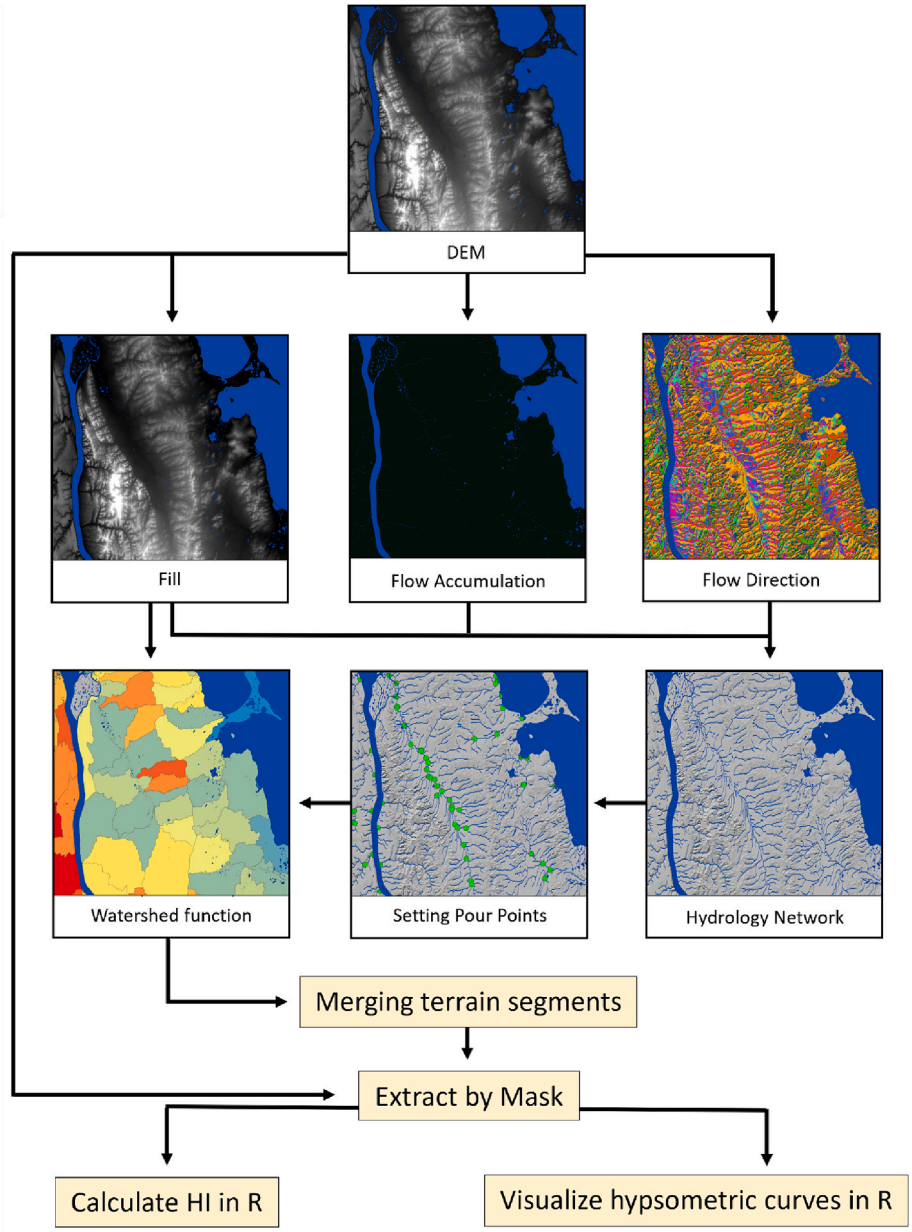

Fig. 4. Workflow of the hypsometric analysis. Hydrological analyses are used to delineate terrain segments from the study area, and their hypsometric integral values are subsequently analyzed in R (R Core Team, 2021).

topography in the area comprises fragments of the Edoma plains shaped by permafrost processes (Bykovsky Peninsula, Muostakh Island, fragment of an Edoma plain along the coast of the Buor-Khaya Bay, class 10, Fig. 7), while fluvial topography is represented by the Lena Delta, its floodplain and extensive terraces, and deltas of small rivers (class 11, Fig. 7).

5.2. Lineaments

A total of 873 lineaments are manually extracted, with lengths ranging from 1.5 km (set as minimum length) to 63.2 km (Fig. 8). Most lineaments are between 1.5 km and 9.7 km in length. A rose diagram is used to record the frequency of lineament orientations, which show a general NE-SW (040°–080°) striking direction (Fig. 8). Subsidiary lineament orientations are E-W (080°–100°), NNE-SSW (020°–040°), and NNW-SSE (160°–180°). The lowest density of lineaments is observed in the Chekanovsky Sector.

Lineaments extracted automatically by the LINE algorithm are shown in Figs. S3 and S4 of the Supplementary Material. The results based on the ArcticDEM DSMs (Suppl. Fig. S3) reveal a large quantity of relatively small and dense lineaments with a general NE-SW orientation. In contrast, lineaments derived from Sentinel-2 satellite imagery using the LINE algorithm (Suppl. Fig. S4) are fewer in quantity, larger in length, and more homogenously distributed. The lineaments extracted by LINE are dominantly NE-SW or N-S oriented.

5.3. Hypsometry

The HI values for the terrain segments in both the Kharaulakh and Chekanovsky sectors range from 0.07 to 0.68. These values are categorized into eight separate classes (Fig. 9). The hypsometric curves of all terrain segments are grouped into four plots corresponding to the subsectors: northern, southern, and central Kharaulakh sub-sectors, and the Chekanovsky Sector (i.e., western sub-sector), for easier comparison.

Areas of low HI values (0.07 to 0.30) are observed particularly in the central Kharaulakh sub-sector along the Buor-Khaya coast and in the

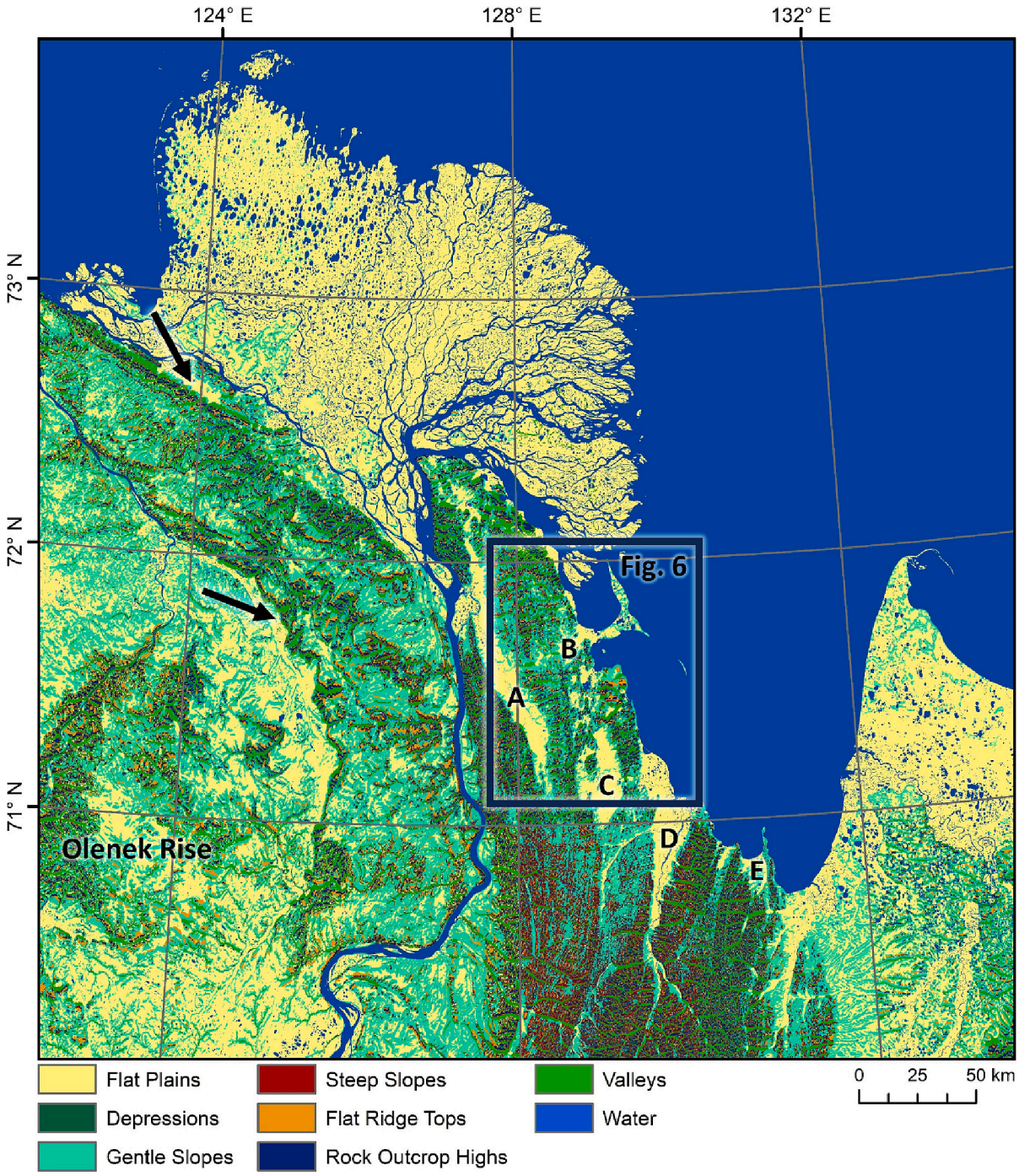

Fig. 5. Terrain classification of M1, utilizing 22 TanDEM-X 30 m DEMs. Cenozoic depressions: (A) Kengdei, (B) Khorogor, (C) Kunga, (D) Kharaulakh, (E) Naiba. The upper arrow indicates a long linear valley that appears to align with associated faults of the Olenek Sector of the highly active Lena-Anabar Segment. The lower arrow marks the location of a prominent valley that runs in a northwest-southeast direction and seems to delineate the boundary between the Cretaceous Chekanovsky Ridge to the east and the Jurassic sedimentary cover of the Siberian Craton to the west.

Kengdei Depression. Moderate HI values (0.30 to 0.45) are predominantly located in the southern Kharaulakh sub-sector, but also in the central northern Kharaulakh sub-sector. High HI values (0.45 to 0.68) are dominant in the Chekanovsky Sector, i.e., western sub-sector. The hypsometric curve plots help to illustrate the hypsometric differences among the four sub-sectors. Hypsometric curves of terrain segments for the central Kharaulakh sub-sector are mostly concave, while hypsometric curves in the southern and northern sub-sectors are S-shaped, and in the western sub-sector they are mostly convex (Fig. 9).

6. Discussion

Assessment of morphometric landscape parameters, alongside lineament analysis, reveals a correlation between modern topography and both geological structures and neotectonic activity. Since for this study, only lineaments exceeding 1.5 km in length are considered, widespread periglacial features are not relevant and excluded from the discussion. Additionally, since the Kharaulakh and Chekanovsky sectors were not covered by an ice sheet since the Late Saalian glaciation (Hubberten et al., 2004; Svendsen et al., 2004; Stauch and Lehmkuhl, 2010), no

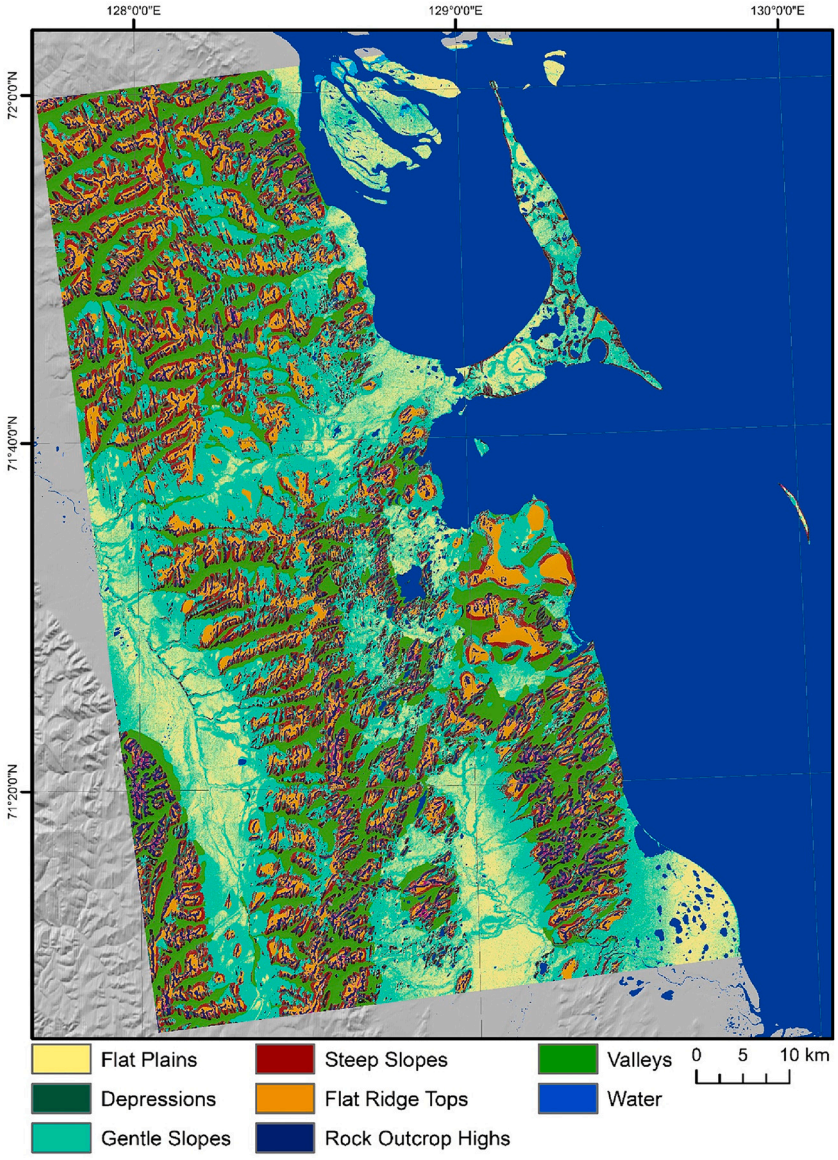

Fig. 6. Terrain classification of M2, utilizing 4 ArcticDEM DSMs. Background: Hillshade map.

morphologically prominent moraines are present. Therefore, we assume that the selected and analyzed lineaments (Fig. 8) are structural. The patterns of their distribution, imposed on information about geology, tectonics, and seismicity of the area, contribute to the understanding of the stress field during the formation of these lineaments, the potential stages of landscape formation, and the origin of distinct topography classes identified during the geomorphological analysis.

The hypsometric integral (HI) and its spatial distribution (Fig. 9) offer insights into possible directions of vertical crustal movements or the relationship between geological composition and modern topography, complemented by information on elevations (Suppl. Fig. S5), geology (Fig. 8), and geomorphology (Fig. 7). Although the interpretation of HI is not straight-forward and might need additional data or analysis, high values generally indicate potentially unstable areas undergoing active uplift and are relatively young. Conversely, low values are often associated with landscapes that are older, more eroded, and possibly less influenced by tectonic activity (e.g., El Hamdouni et al., 2008). Together with the results of the BTM terrain classification, HI values help reveal patterns of regional neotectonic activity or geological control of the topography.

The Chekanovsky Sector west of the Lena River, primarily composed of Mesozoic sandstones, constitutes part of the stable Siberian Craton and has not undergone Mesozoic folding (Borisova and Gercheva, 2016; Prokopiev et al., 2001). The sector is characterized by epiplatform block mountains and hills (Fig. 10 a, geomorphological classes 1 and 2, see Fig. 7), adjacent to the contact zone with the Verkhoyansk fold-and-thrust-belt. These low mountains up to 400–500 m a.s.l. were formed by block movements along faults and erosion in the valleys set along fractures and faults. The BTM terrain classification describes this area as a flat to gently sloped plateau, dissected by steep valleys (Fig. 5). Towards the west, the elevation drops by ~200-meters along the erosional escarpment of the Chekanovsky Ridge, potentially representing the ancient Lena River valley during glacial periods, a hypothesis also proposed by previous research from Puminov (1960). The epiplatform hills and mountains are separated from the eastward lying structures of the Verkhoyansk fold-and-thrust belt by the contact area with the Siberian Craton, topographically characterized by gentle slopes (Fig. 10 b, geomorphological class 3, see Fig. 7) at the pediment of the mountains descending towards the Lena River.

The central Chekanovsky Sector is characterized by prominent NE-SW trending lineaments, (Fig. 8). In the northern Chekanovsky Sector, lineaments follow predominantly NNW-SSE and NW-SE directions,

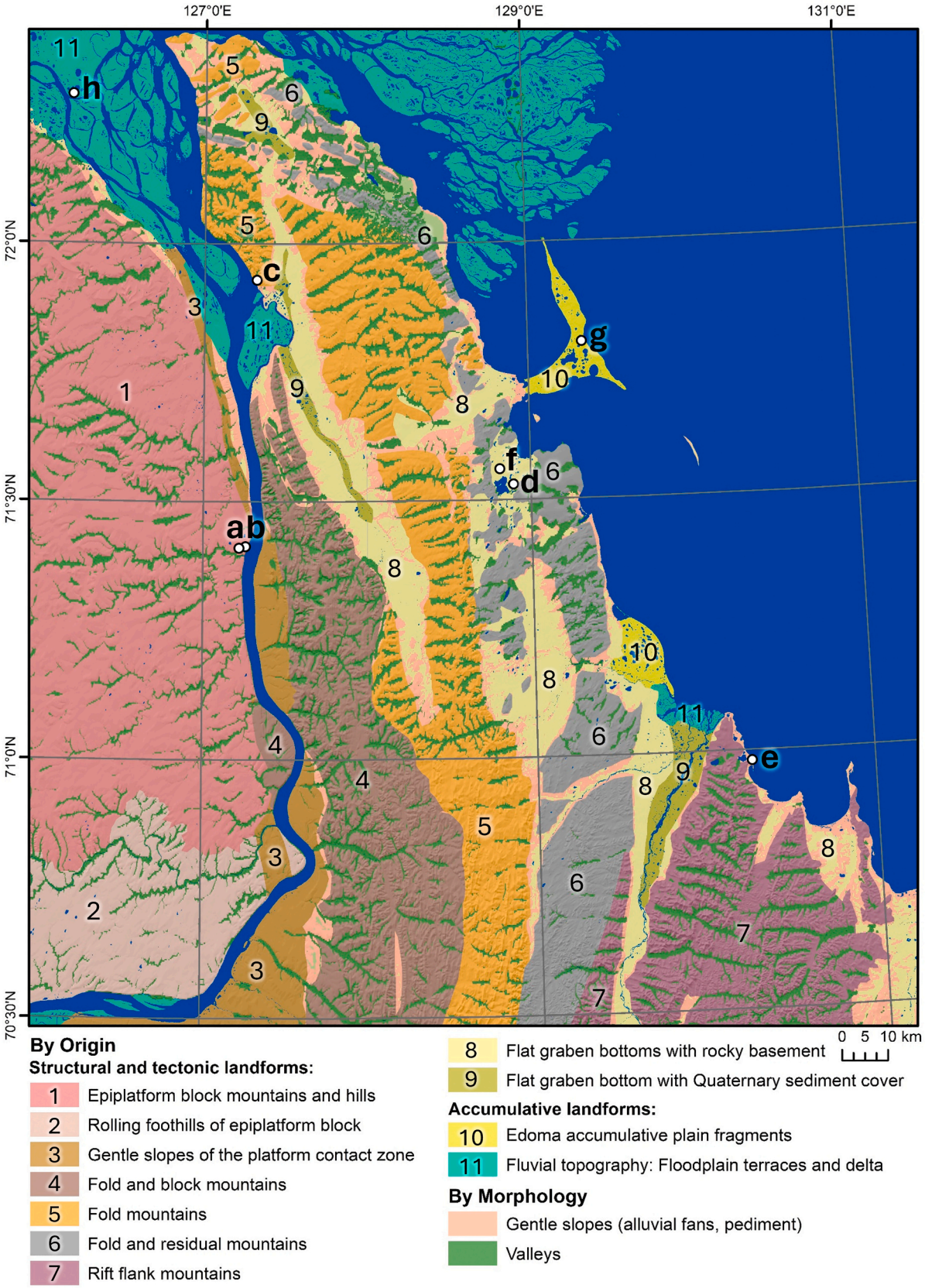

Fig. 7. Geomorphological map of the study area. Landforms are categorized based on their origin; gentle slopes and valleys are separately selected based on morphology only. (a–h) Locations of photographs in Fig. 10.

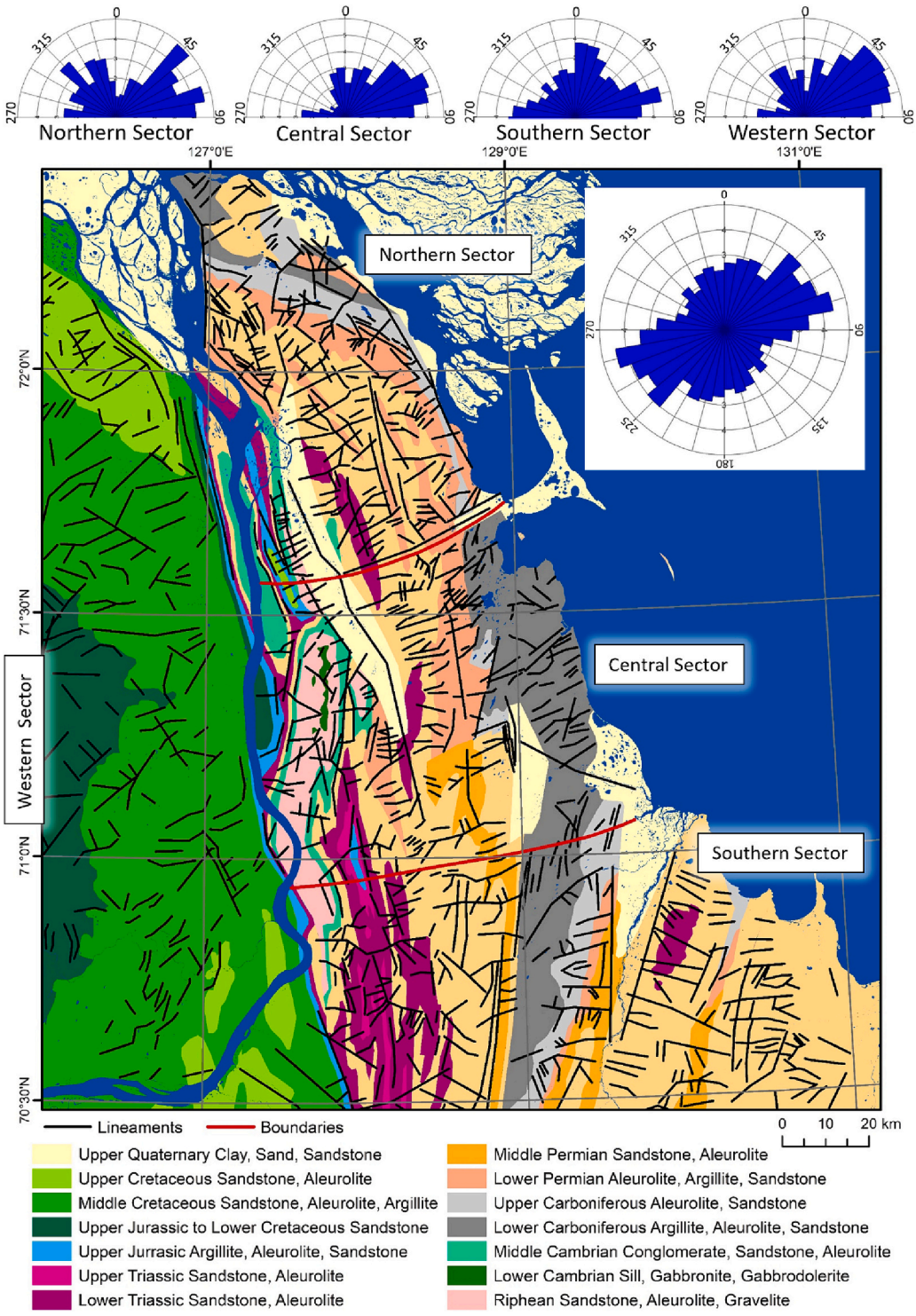

Fig. 8. Lineaments and geology of the Kharaulakh and Chekanovsky sectors. The rose diagrams show the orientation of the lineaments for each sub-sector (top) and the entire study area. The geological classification is modified after Borisova and Gercheva, 2016.

resembling features that could be interpreted as the eastern prolongation of the Lena-Anabar structural suture (see Fig. 1). Most lineaments align with fluvially incised valleys, displaying a meandering form (Fig. 10 a). This suggests that there are relatively few inherited fractures and faults within the Cretaceous platform sandstones that could focus erosion and incision of valleys. The valley networks in the western Chekanovsky Sector exhibit a dendritic pattern, indicating flat-lying rocks or sediments with few structural weaknesses, which is proved by geological data (Fig. 8). Carved by westward-flowing rivers and creeks, the valleys are indicative of a retrogressive erosion process. A prominent, continuous valley extending from the Olenek River in a northwest to southeast direction along the Chekanovsky Ridge (Fig. 5) seems to delineate the erosional escarpment, exposing the Jurassic sedimentary cover. Younger contributary valleys along the Lena River display deeper incisions and are predominantly oriented eastward (Suppl. Fig. S2). Notably, no river terraces are observed along their slopes (Fig. 10 a), implying that incision/uplift in this area likely occurred continuously rather than in distinct stages until recent times. This suggests, in our

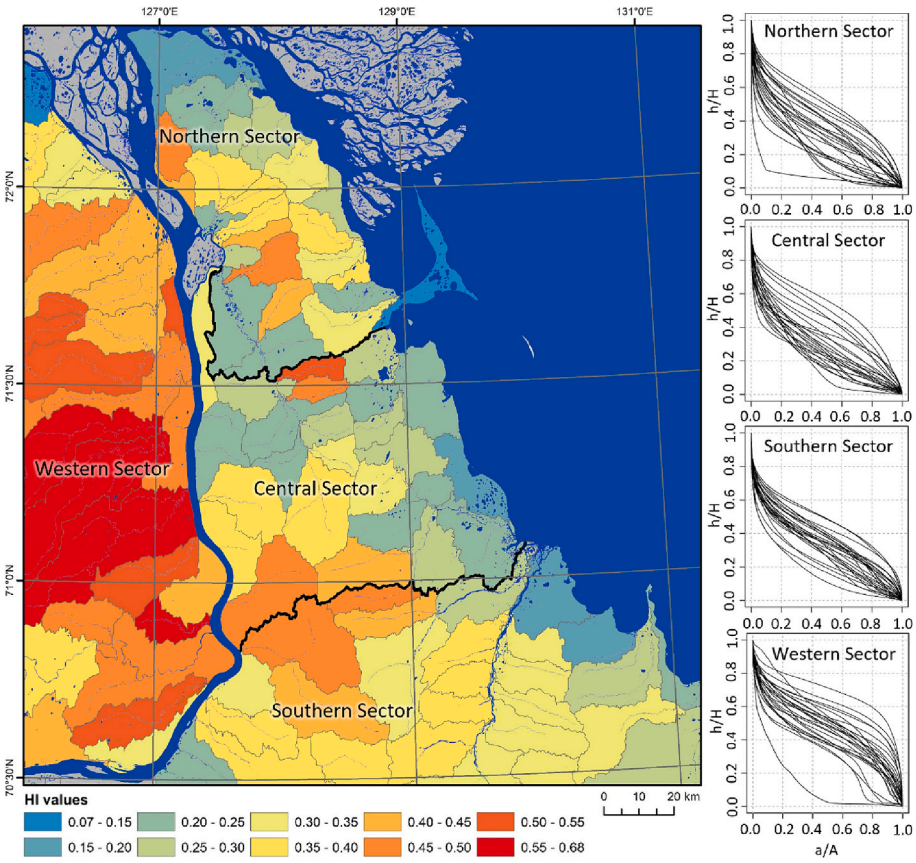

Fig. 9. Hypsometric integral (HI) values for each of the 105 terrain segments with the respective hypsometric curves for the four sub-sectors.

view, a very recent and ongoing uplift or westward tilting of the Chekanovsky Ridge.

These assumptions align with the highest HI values in the study area (ranging from 0.40 to 0.68, see Fig. 9) in the Chekanovsky Sector. This may be partly attributed to the homogeneous, untectonized structure of the Cretaceous platform sandstones. However, recent uplift and potential tilting might have a larger influence on the HI values. Situated within the southwestern boundary of the LSM (Fig. 1), the Chekanovsky Sector likely experiences compression conditions, resulting from extensional rifting processes confined to the eastern LSM boundary (Avetisov, 2000; Imaev et al., 2018; Imaeva et al., 2020). Geological and geophysical research supports this, showing increased uplift of the western Lena Delta (Bolshiyanov et al., 2019). According to Sim et al. (2018) and Imaeva et al. (2018, 2019), the Chekanovsky Sector exhibits increased neotectonic activity, although more intense activity is assumed in the Kharaulakh Sector.

The topography of the Kharaulakh Sector, comprising the eastern part of the study area, features several parallel NNW-SSE trending low ridges (Tuora-Sis Ridge, Kharaulakh Ridge, Primorsky Ridge, Naiba Ridge, see Figs. 1 and 7). These low ridges, characterized by sharp crests and sometimes steep slopes (Fig. 10 c), inherit the folded structure of the Verkhoyansk fold-and-thrust belt from the Mesozoic era. The difference in their topography results from both different neotectonic activity and differences in rock resistance, influenced by bedding, geological composition, and jointing of the rocks exposed in each ridge. Generally, within the Kharaulakh Sector, the individual defined geomorphological classes predominantly align with the strike of the fold-and-thrust belt, suggesting, at least in part, lithological or fold-belt-related tectonic control. The same applies for longer lineaments of the N-S or NNW-SSW directions imposing the general orientation of the Verkhoyansk fold system. Shorter lineaments (<10 km) are numerous and have a preferred ENE-WSW to NE-SW orientation (Fig. 8). This orientation is perpendicular to the strike of the lithological units and the strike of the fold belt, which strongly indicates their inheritance from their original depositional setting and/or the later compressional tectonics during the formation of the Verkhoyansk fold-and-thrust belt. At present, many of these WSW-ENE to SW-NE orientated lineaments are closely related to valleys and ridges, as can be seen in the BTM terrain classification for the Kharaulakh Sector (Figs. 5 and 6), indicating that these inherited structures serve as weak zones, facilitating easier erosion and incision by creeks and rivers. A few extended lineaments or chains of lineaments are also oriented NE-SW, perpendicular to the fold belts strike, like those observed along the Korogor Valley between the northern and southern Kharaulakh sub-sectors (Fig. 8). These are likely derived from inherited fractures or fault zones but most likely have experienced neotectonic reactivation, as indicated by increased seismicity along these structures (Imaev et al., 2000; Fujita et al., 1990a; Grosse et al., 2007).

Long N-S and NNE-SSW oriented valleys and lineaments in the southern Kharaulakh sub-sector are associated with a system of N-S strike-slip faults that extend for approximately 200 km from the Kunga Graben in the north to the southern foothills of the Kharaulakh Ridge (Imaev et al., 2018; Imaeva et al., 2019). However, many of these N-S or NNW-SSE oriented lineaments coincide with the strike of graben structures formed during the early Cenozoic (Imaeva et al., 2016). The same pattern applies to grabens with flat rocky basement or a very thin Quaternary sediment cover (Fig. 10 f), classified by the BTM as mainly flat plains, and partly gentle slope areas (Figs. 5 and 6). These structures, although partly inherited from the older Mezozoic folds and faults, were re-activated or formed in the Cenozoic to recent times after the opening of the Arctic Ocean and the spreading on the Gakkel Ridge (Chapman and Solomon, 1976; Grachev, 1973; Fujita et al., 1990b), which lead to extension on the Laptev Shelf continental margin and formation of the Laptev Sea rift system (Drachev, 2000; Drachev et al., 2003). The coasts of the Buor-Khaya Bay situated on the flanks of one of the rifts of the

Fig. 10. Photographs from the field to illustrate selected geomorphological classes. Locations are marked on Fig. 7. Geomorphological classes: (a) Epiplatform block mountains, valley fragment; (b) Gentle slopes of the platform contact zone descending to the Lena River (seen at the foothills of the fold and block mountains in the background); (c) Fold mountains, valley fragment; (d) Fold and residual mountains, Lake Sevastian; (e) Rift flank mountains (in the background); (f) Flat graben bottoms with rocky basement; (g) Edoma accumulative plain, Bykovsky Peninsula; (h) Floodplain terrace, Lena Delta.

Laptev Sea rift system (Franke et al., 2001), were also subject to that ongoing regional deformation. In particular, the faults bounding the Kharaulakh and Naiba grabens (Fig. 5) form a northeastern and sub-latitudinal system, aligning well with fault systems of the Ust' Lena Rift (Fig. 1) on the Laptev Sea shelf (Sekretov, 2002; Imaeva et al., 2016). The association of graben and lineament formation with the extensional rift setting is further supported by data on modern earthquakes, with predominantly strike-slip and extension mechanisms occurring along this seismic zone (Imaev et al., 2000).

The HI values in the Kharaulakh Sector exhibit considerable variability, suggesting that the trends of vertical crustal movements may have differed during the Cenozoic to recent times, and that lithological variations here also significantly influence topographical differentiation. Areas of accumulative topography, such as the Lena Delta (Fig. 10 g) and young depositional Edoma plains like the Bykovski Peninsula (Fig. 10 h), as well as the catchment areas along the northern and eastern coasts, are typified by flat to gently sloped terrain. These areas act as depositional sites for sediments eroded from the Kharaulakh and Primorsky ridges, leading to low HI values, indicative of relative neotectonic subsidence. Low HI values (<0.3) were previously documented for the depressions related to the Eger Rift, Central Europe, by Andreani et al. (2014), whereas the uplifted rift shoulders and nearby plateaus show HI values of 0.5 to 0.7. Specifically, the central Kharaulakh subsector exhibits low HI values ($\sim$0.15 to 0.30) along the Buor-Khaya coast. This region experiences increased seismic activity (generally magnitude <3.9) and high neotectonic activity (Imaeva et al., 2019). This suggests that the low observed HI values along the coasts, as well as near the Cenozoic Kengdei, Kunga, and Sogo grabens, may be an expression of the Cenozoic and modern extension and subsidence. It is likely that the extension in the western grabens has already ceased, while it continues along the coast of Buor-Khaya Bay, as indicated by seismic activity (Avetisov, 2000; Imaev et al., 2018; Imaeva et al., 2020).

Nonetheless, variations in the HI values in the Kharaulakh Sector also derive from differing geological influences on topographical formation. The Primorsky Ridge bordering Lake Sevastian and the Buor-Khaya Bay features low elevations (<400 m above sea level) with sharp edges formed along lineaments presumably of tectonic origin, as well as low HI values (0.15–0.25). The carboniferous siltstones composing Primorsky Ridge were displaced by the Sevast'yanov overthrust (Imaev et al., 2018), and exhibit heavy cleavage and high potential for erosion (Fig. 10 d), contributing to the region's lower relief and HI values.

The folded rift flank mountains bordering the Naiba Rift (class 7 and southern part of class 6, Fig. 7) exhibit higher elevations than the Primorsky Ridge (up to 700 m), along with average HI values (0.30–0.40). This could be attributed to the greater rock resistance compared to the Primorsky Ridge. It is probable that this area underwent extension during the neotectonic period, along with block rift movements, resulting in the subsidence of the central rift part accompanied by relative uplift of the mountains on its flanks. In contrast, the northern Kharaulakh Ridge features medium to high HI values (0.30 to 0.50) especially towards the west (Fig. 9), owing to the deeply incised NE-SW and E-W oriented linear valleys leading into the Kengdei Graben with elevation differences of ~200 m. These elevated HI values might indicate ongoing uplift and neotectonic activity in the northern Kharaulakh Ridge, as already indicated by Imaeva et al. (2018), potentially with a reactivation of thrust faults of the Late Mesozoic Verkhoyansk fold-and-thrust belt resulting from compressional conditions. Elevated HI values were previously interpreted as signs of young uplift and neotectonic activity in the Eger Rift region (Andreani et al., 2014) and the Tatra Mountains (Buczek and Górnik, 2020).

The southern parts of the Kharaulakh and Tuora-Sis ridges, characterized by faulted block ridges and folding (Fig. 7) inherited from the Verkhoyansk orogeny (Borisova and Gercheva, 2016; Prokopiev et al., 2001), are situated at present within a region of compression southward of the rotation pole at the Eurasian and North American plate boundary (Fig. 1). Medium to high HI values (~0.30 to 0.50) are observed here, with the deepest incisions (~300 to 800 m) and largest elevation differences of the study area. Seismicity catalogues (e.g., Fujita et al., 2009; Imaeva et al., 2018, 2019, 2020) show the strongest recorded earthquakes (Ms 6.1–7.0) in close vicinity. Imaeva et al. (2018) reported a general uplift tendency of 0–8 mm/yr for this area. Moreover, Imaeva et al. (2019) proposed an increased geodynamic activity of neotectonic structures. That would agree with our interpretation, that the elevated HI values in the study area are, at least in part, related to neotectonic activity and uplift.

7. Conclusions

The analysis of morphostructural, geological, and geomorphological characteristics of the Kharaulakh and Chekanovsky sectors, reveals the interplay between extensional and compressional features at the junction of the Laptev Sea Rift System, Verkhoyansk fold-and-thrust belt, and the stable Siberian Craton. Employing the Benthic Terrain Modeler enables a semi-automatic terrain classification, facilitating the categorization of landforms based on their structural, tectonic, accumulative, or erosive characteristics, as well as their spatial distribution and morphological features. Lineament analysis identified 873 features across the Kharaulakh and Chekanovsky sectors.

The highest hypsometric integral values in the region were revealed for the Chekanovsky Sector, situated within the stable Siberian Craton. Its topography is characterized by epiplatform low block mountains significantly dissected by faults. These high HI values derive from compressional conditions induced by rifting processes along the eastern Laptev Sea Microplate boundary.

The Kharaulakh Sector, situated within the Verkhoyansk fold-and-thrust belt, exhibits topographical variations influenced by lithology, geological, and tectonic factors, as well as neotectonic movements. Variations in rock resistance contribute to differingl erosion rates, resulting in relatively low topography and hypsometric indices in areas composed by highly cleavages Carboniferous siltstones and sandstones, such as Primorsky Ridge. The NNW-SSE orientation of long lineaments, imposing the structures of the Verkhoyansk fold-and-thrust belt, suggests that the topography aligns with the folding and faulting processes of the Mesozoic era. However, this inherited structure has experienced reactivation during the neotectonic period, likely influenced by extension and rift formation on the Laptev Sea shelf, leading to renewed activity along N-S and NE-SW faults, manifested as lineaments. This influence has caused recent extension and both upward and downward block movements in coastal areas of the Buor-Khaya Bay (Naiba Ridge, Primorsky Ridge), while ridges further to the west (Tuora-Sis Ridge) experience higher compression and more active uplift. This neotectonic activation has also contributed to the formation of grabens dissecting the fold and block mountains.

CRediT authorship contribution statement

Jakob S. Hamann: Writing – review & editing, Writing – original draft, Visualization, Validation, Supervision, Software, Resources, Project administration, Methodology, Investigation, Funding acquisition, Formal analysis, Data curation, Conceptualization. **Alisa V. Baranskaya:** Writing – review & editing, Validation, Resources, Methodology, Formal analysis, Data curation. **Wolfram H. Geissler:** Writing – review & editing, Validation, Supervision, Resources, Investigation, Funding acquisition, Formal analysis, Data curation, Conceptualization. **Boris V. Baranov:** Writing – review & editing, Validation, Investigation, Formal analysis, Data curation. **Nikolay V. Tsukanov:** Writing – review & editing, Validation, Resources, Formal analysis, Data curation.

Declaration of competing interest

The authors declare that they have no known competing financial interests or personal relationships that could have appeared to influence the work reported in this paper.

Data availability

Data will be made available on request.

Acknowledgements

We thank Christian Brandes for his valuable insights and discussions on the manuscript, as well as to Bennet Juhls for support with remote sensing and data availability. Boris Baranov and Nikolay Tsukanov acknowledge support from the Institute of Oceanology Russian Academy of Sciences, project no. FMMG-2023-0005. Alisa Baranskaya acknowledges support from the RSCF project 22-77-10031. We also thank two anonymous reviewers for their constructive comments.

Appendix A. Supplementary data

Supplementary data to this article can be found online at https://doi.org/10.1016/j.geomorph.2024.109228.

References

Ahmadi, H., Pekkan, E., 2021. Fault-based geological lineaments extraction using remote sensing and GIS - a review. Geosciences 11 (5), 183. https://doi.org/10.3390/geosciences11050183.

Andreani, L., Stanek, K.P., Gloaguen, R., Krentz, O., Domínguez-González, L., 2014. DEM-based analysis of interactions between tectonics and landscapes in the Ore Mountains and Eger Rift (East Germany and NW Czech Republic). Remote Sens. (Basel) 6 (9), 7971–8001.

Andreev, V.S., Dovydenko, G.M., Egorov, A., Kirichenko, V.G., 1981. Godsudarstvennaja Geologitscheskaja Karta SSSR, 1:200,000, Veryojanskaja Serjia, R-52-IX, X

[Geological map of the USSR, 1:200,000, Verkhoyanskaya Series, R-52-IX, X]. Ministerstvo Geologii SSSR [Ministry of Geology of the USSR].
Assatse, W.T., Nouck, P.N., Tabod, C.T., Akame, J.M., Biringanine, G.N., 2016. Hydrogeological activity of lineaments in Yaoundé Cameroon region using remote sensing and GIS techniques. Egypt. J. Remote Sens. Space Sci. 19 (1), 49–60. https://doi.org/10.1016/J.EJRS.2015.12.006.
Avetisov, G.P., 2000. Once Again on the Earthquakes of the Laptev Sea, Geological–Geophysical Features of the Lithosphere of the Arctic Region, 3. Ministry of Natural Resources of the Russian Federation, All-Russia Research Institute for Geology and Mineral Resources of the World Ocean, pp. 104–114 (In Russian).
Baranskaya, A., 2013. The latest tectonic movements in the transitional extension settings on the coasts of Buor Kaya Bay, Laptev Sea [Poster presentation]. In: European Geosciences Union General Assembly 2013, Vienna, Austria.
Bidzhiev, R.A., 1970. Godsudarstvennaja Geologitscheskaja Karta SSSR, 1:200,000, Nijnielenskaja Serjia, R-52-VII, VIII [Geological map of the USSR, 1:200,000, Lower Lena Series, R-52-VII, VIII]. Ministerstvo Geologii SSSR [Ministry of Geology of the USSR].
Bijiyev, R.A., Gorshkova, R., 1975. Godsudarstvennaja Geologitscheskaja Karta SSSR, 1:200,000, Veryojanskaja Serjia, R-52-III, IV [Geological map of the USSR, 1:200,000, Verkhoyanskaya Series, R-52-III, IV]. Ministerstvo Geologii SSSR [Ministry of Geology of the USSR].
Bolshiyanov, D.Y., Aksenov, A.O., Makarov, A.S., Lazareva, E.I., Pravkin, S.A., Cherezova, A.A., Grigoriev, M.N., 2019. Geomorphological structure and neotectonics of the Lena delta. Arctic Antarctic Res. 65 (2), 186–200. https://doi.org/10.30758/0555-2648-2019-65-2-186-200.
Bonetto, S., Facello, A., Ferrero, A.M., Umili, G., 2015. A tool for semi-automatic linear feature detection based on DTM. Comput. Geosci. 75, 1–12. https://doi.org/10.1016/j.cageo.2014.10.005.
Borisova, T.P., Gercheva, M.V., 2016. State Geological Map of the Russian Federation, Third Generation, Verkhoyano-Kolymskaya Series: Geological Map of Quaternary Formations, Scale 1:1,000,000, Sheet R-52 (Tiksi). [Map]. Cartographic Factory of VSEGEI.
Brandes, C., Tanner, D.C., 2020. Fault mechanics and earthquakes. In: Tanner, D., Brandes, C. (Eds.), Understanding Faults: Detecting, Dating, and Modeling. Elsevier, pp. 11–80.
Buczek, K., Górnik, M., 2020. Evaluation of tectonic activity using morphometric indices: case study of the Tatra Mts. (Western Carpathians, Poland). Environmental Earth Sciences 79 (8), 176. https://doi.org/10.1007/s12665-020-08912-9.
Chapman, M.E., Solomon, S.C., 1976. North American-Eurasian plate boundary in northeast Asia. J. Geophys. Res. 81 (5), 921–930. https://doi.org/10.1029/JB081I005P00921.
De Reu, J., Bourgeois, J., Bats, M., Zwertvaegher, A., Gelorini, V., De Smedt, P., Chu, W., Antrop, M., De Maeyer, P., Finke, P., Meirvenne, M., Verniers, J., Crombe, P., 2013. Application of the topographic position index to heterogeneous landscapes. Geomorphology 186, 39–49. https://doi.org/10.1016/j.geomorph.2012.12.015.
Drachev, S.S., 2000. Laptev Sea rifted continental margin: modern knowledge and unsolved questions. Polarforschung 68, 41–50.
Drachev, S.S., Kaul, N., Beliaev, V.N., 2003. Eurasia spreading basin to Laptev Shelf transition: structural pattern and heat flow. Geophys. J. Int. 152 (3), 688–698. https://doi.org/10.1046/j.1365-246X.2003.01882.x.
Drăguţ, L., Blaschke, T., 2006. Automated classification of landform elements using object-based image analysis. Geomorphology 81 (3–4), 330–344. https://doi.org/10.1016/J.GEOMORPH.2006.04.013.
Drusch, M., Del Bello, U., Carlier, S., Colin, O., Fernandez, V., Gascon, F., Hoersch, B., Isola, C., Laberinti, P., Martimort, P., Meygret, A., Spoto, F., Sy, O., Marchese, F., Bargellini, P., 2012. Sentinel-2: ESA's Optical High-Resolution Mission for GMES Operational Services. Remote Sens. Environ. 120, 25–36. https://doi.org/10.1016/J.RSE.2011.11.026.
Duan, Y., Pei, X., Zhang, X., 2022. The hypsometric integral based on digital elevation model for the area west of Lvliang Mountains in Loess Plateau, Shanxi, China. Front. Earth Sci. 10, 1–14. https://doi.org/10.3389/feart.2022.827836.
El Hamdouni, R., Irigaray, C., Fernández, T., Chacón, J., Keller, E.A., 2008. Assessment of relative active tectonics, southwest border of the Sierra Nevada (southern Spain). Geomorphology 96 (1–2), 150–173. https://doi.org/10.1016/J.GEOMORPH.2007.08.004.
Elmahdy, S., Mohamed, M., Ali, T., 2019. Automated detection of lineaments express geological linear features of a tropical region using topographic fabric grain algorithm and the SRTM DEM. Geocarto Int. 36 (1), 76–95. https://doi.org/10.1080/10106049.2019.1594393.
Erdey-Heydorn, M., 2008. An ArcGIS seabed characterization toolbox developed for investigating benthic habitats. Mar. Geod. 31 (4), 318–358. https://doi.org/10.1080/01490410802466819.
Fairbanks, R., 1989. A 17,000-year glacio-eustatic sea level record: influence of glacial melting rates on the Younger Dryas event and deep-ocean circulation. Nature 342 (6250), 637–642. https://doi.org/10.1038/342637a0.
Farhan, Y., Elgaziri, A., Elmaji, I., Ali, I., 2016. Hypsometric analysis of Wadi Mujib-Wala watershed (Southern Jordan) using remote sensing and GIS techniques. Int. J. Geosci. 7 (2), 158–176. https://doi.org/10.4236/ijg.2016.72013.
Faulkner, D.R., Mitchell, T.M., Jensen, E., Cembrano, J., 2011. Scaling of fault damage zones with displacement and the implications for fault growth processes. J. Geophys. Res. Solid Earth 116. https://doi.org/10.1029/2010JB007788.
Franke, D., Hinz, K., Oncken, O., 2001. The Laptev sea rift. Mar. Pet. Geol. 18 (10), 1083–1127. https://doi.org/10.1016/S0264-8172(01)00041-1.
Fujita, K., Cook, D.B., Hasegawa, H., Forsyth, D., Wetmiller, R., 1990a. Seismicity and focal mechanisms of the Arctic region and the North American plate boundary in Asia. In: Grantz, A., Johnson, L., Sweeney, J.F. (Eds.), The Arctic Ocean Region, Vol. L. Geological Society of America, pp. 79–100.
Fujita, K., Cambray, F.W., Velbel, M.A., 1990b. Tectonics of the Laptev Sea and Moma rift systems, northeastern USSR. Mar. Geol. 93, 95–118. https://doi.org/10.1016/0025-3227(90)90079-Y.
Fujita, K., Koz'min, B., Mackey, K., Riegel, S., McLean, M., Imaev, V., 2009. Seismotectonics of the Chersky Seismic Belt, eastern Sakha Republic (Yakutia) and Magadan District, Russia. Stephan Mueller Special Publication Series 4, 117–145. https://doi.org/10.5194/smsps-4-117-2009.
Gioia, D., Danese, M., Corrado, G., Di Leo, P., Minervino Amodio, A., Schiattarella, M., 2021. Assessing the prediction accuracy of geomorphon-based automated landform classification: an example from the ionian coastal belt of southern Italy. ISPRS Int. J. Geo Inf. 10 (11), 725. https://doi.org/10.3390/ijgi10110725.
Goes, E., Brown, C., Araújo, T., 2019. Geomorphological Classification of the Benthic Structures on a Tropical Continental Shelf. Front. Mar. Sci. 6, 47. https://doi.org/10.3389/fmars.2019.00047.
Gogina, N.I., 1975. Godsudarstvennaja Geologitscheskaja Karta SSSR, 1:200,000, Nijnielenskaja Serjia, S-52-XXXI, XXXII [Geological map of the USSR, 1:200,000, Lower Lena Series, S-52-XXXI, XXXII]. Ministerstvo Geologii SSSR [Ministry of Geology of the USSR].
Gogina, N.I., Gorschkova, E.R., Groschin, S.M., 1971. Godsudarstvennaja Geologitscheskaja Karta SSSR, 1:200,000, Nijnielenskaja Serjia, R-52-I, II [Geological map of the USSR, 1:200,000, Lower Lena Series, R-52-I, II]. Ministerstvo Geologii SSSR [Ministry of Geology of the USSR].
Grachev, A.F., 1973. Moma continental rift (northeast SSSR). Geofizicheskiye metody razvedki v Arktike 56–75 (in Russian).
Grachev, A.F., Demenitskaya, R.M., Karasik, A.M., 1970. The Mid-Arctic Ridge and its continental continuation. Geomorphology 1, 30–32.
Grosse, G., Schirrmeister, L., Siegert, C., Kunitsky, V., Slagoda, E., Andreev, A., Dereviagyn, A., 2007. Geological and geomorphological evolution of a sedimentary periglacial landscape in Northeast Siberia during the Late Quaternary. Geomorphology 86 (1–2), 25–51. https://doi.org/10.1016/J.GEOMORPH.2006.08.005.
Henderson, D.B., Ferrill, D.A., Clarke, K.C., 1996. Mapping geological faults using image processing techniques applied to hill-shaded digital elevation models. In: Proceedings of the IEEE Southwest Symposium on Image Analysis and Interpretation, pp. 240–245. https://doi.org/10.1109/IAI.1996.493760.
Hubberten, H., Andreev, A., Astakhov, V.I., Demidov, I., Dowdeswell, J.A., Henriksen, M., Hjort, C., Houmark-Nielsen, M., Jakobsson, M., Larsen, E., Lunkka, J. P., Lysså, A., Mangerud, J., Möller, P., Saarnisto, M., Schirrmeister, L., Sher, A.V., Siegert, C., Siegert, M.J., Svendsen, J.I., 2004. The periglacial climate and environment in northern Eurasia during the Last Glaciation. Quat. Sci. Rev. 23 (11−13), 1333–1357. https://doi.org/10.1016/J.QUASCIREV.2003.12.012.
Huggett, R., Shuttleworth, E., 2022. Fundamentals of Geomorphology. Taylor & Francis.
Imaev, V.S., Imaeva, L.P., Koz'min, B.M., 2000. Seismotectonics of Yakutia. GEOS 227 (in Russian).
Imaev, V., Imaeva, L., Smekalin, O., Chipizubov, A., Ovsyuchenko, A., Kolodeznikov, I., 2018. Neotectonics of the Kharaulakh sector of the Laptev Shelf. Russ. Geol. Geophys. 59 (7), 813–826. https://doi.org/10.1016/J.RGG.2018.07.007.
Imaeva, L.P., Kolodeznikova, I.I., 2017. Seismotectonics of the north-eastern sector of the Russian Arctic. Siberian Branch of the Russian Academy of Sciences 134 (in Russian).
Imaeva, L., Imaev, V., Mel'nikova, V., Koz'min, B., 2016. Recent structures and tectonic regimes of the stress–strain state of the Earth's crust in the northeastern sector of the Russian Arctic region. Geotectonics 50 (6), 535–552. https://doi.org/10.1134/S0016852116060030.
Imaeva, L., Gusev, G., Imaev, V., Mel'nikova, V., 2017. Neotectonic activity and parameters of seismotectonic deformations of seismic belts in Northeast Asia. J. Asian Earth Sci. 148, 254–264. https://doi.org/10.1016/J.JSEAES.2017.09.007.
Imaeva, L.P., Imaev, V.S., Koz'min, B.M., 2018. Seismotectonic activation of modern structures of the Siberian Craton. Geotectonics 52, 618–633. https://doi.org/10.1134/S0016852118060031.
Imaeva, L., Imaev, V., Koz'min, B., 2019. Dynamics of the zones of strong earthquake epicenters in the Arctic–Asian seismic belt. Geosciences 9 (4), 168. https://doi.org/10.3390/geosciences9040168.
Imaeva, L.P., Gusev, G.S., Imaev, V.S., 2020. Seismotectonics of the northern sector of the Verkhoyansk fold system (northeast of the Russian Arctic). Natural Resources of the Arctic and Subarctic 25 (2), 5–24. https://doi.org/10.31242/2618-9712-2020-25-2-1.
Javhar, A., Chen, X., Bao, A., Jamshed, A., Yunus, M., Jovid, A., Latipa, T., 2019. Comparison of multi-resolution optical Landsat-8, Sentinel-2 and Radar Sentinel-1 data for automatic lineament extraction: a case study of Alichur Area, SE Pamir. Remote Sensing 11 (7), 778. https://doi.org/10.3390/RS11070778.
Jenness, J., 2006. Topographic position index (tpi_jen.avx) extension for arcview 3.x, v. 1.2. Jenness Enterprises. Available at. http://www.jennessent.com/arcview/tpi.htm.
Jordan, G., Schott, B., 2005. Application of wavelet analysis to the study of spatial pattern of morphotectonic lineaments in digital terrain models. A case study. Remote Sens. Environ. 94 (1), 31–38. https://doi.org/10.1016/J.RSE.2004.08.013.
Lundblad, E., Wright, D., Miller, J., Larkin, E., Rinehart, R., Naar, D., Danahue, B.T., Anderson, S.M., Battista, T., 2006. A benthic terrain classification scheme for American Samoa. Mar. Geod. 29 (2), 89–111. https://doi.org/10.1080/01490410600738021.
Mahmood, S.A., Gloaguen, R., 2012. Appraisal of active tectonics in Hindu Kush: Insights from DEM derived geomorphic indices and drainage analysis. Geosci. Front. 3 (4), 407–428. https://doi.org/10.1016/J.GSF.2011.12.002.
Mallast, U., Gloaguen, R., Geyer, S., Rödiger, T., Siebert, C., 2011. Derivation of groundwater flow-paths based on semi-automatic extraction of lineaments from

remote sensing data. Hydrol. Earth Syst. Sci. 15 (8), 2665–2678. https://doi.org/10.5194/HESS-15-2665-2011.
Masoud, A., Koike, K., 2011. Auto-detection and integration of tectonically significant lineaments from SRTM DEM and remotely-sensed geophysical data. ISPRS J. Photogramm. Remote Sens. 66 (6), 818–832. https://doi.org/10.1016/J.ISPRSJPRS.2011.08.003.
Mokarram, M., Roshan, G., Negahban, S., 2015. Landform classification using topography position index (case study: salt dome of Korsia-Darab plain, Iran). Model. Earth Systems Environ. 1, 40. https://doi.org/10.1007/s40808-015-0055-9.
Muddarisna, N., Yuniwati, E., Masruroh, H., Oktaviansyah, A., 2020. An automated approach using Topographic Position Index (TPI) for Landform mapping (case study: Gede Watershed, Malang Regency, East Java, Indonesia). IOP Conference Series: Earth And Environmental Science 412, 012027. https://doi.org/10.1088/1755-1315/412/1/012027.
Ohmori, H., 1993. Changes in the hypsometric curve through mountain building resulting from concurrent tectonics and denudation. Geomorphology 8 (4), 263–277. https://doi.org/10.1016/0169-555x(93)90023-u.
O'Leary, D., Friedman, J., Pohn, H., 1976. Lineament, linear, lineation: some proposed new standards for old terms. Geol. Soc. Am. Bull. 87 (10), 1463. https://doi.org/10.1130/0016-7606(1976)87<1463:LLLSPN>2.0.CO;2.
Parfenov, L.M., Kuzmin, M.I., 2001. Tectonics, Geodynamics and Metallogeny of the Sakha Republic (Yakutia) (in Russian). MAIK Nauka/Interperiodika.
Parfenov, L.M., Prokopiev, A.V., Gaiduk, V.V., 1995. Cretaceous frontal thrusts of the Verkhoyansk Fold Belt, eastern Siberia. Tectonics 14 (2), 342–358. https://doi.org/10.1029/94TC03088.
Pérez-Peña, J.V., Azañón, J.M., Booth-Rea, G., Azor, A., Delgado, J., 2009. Differentiating geology and tectonics using a spatial autocorrelation technique for the hypsometric integral. J. Geophys. Res. 114 (F2) https://doi.org/10.1029/2008JF001092.
Piloyan, A., Konečný, M., 2017. Semi-automated classification of landform elements in Armenia based on SRTM DEM using K-means unsupervised classification. Quaestiones Geographicae 36 (1), 93–103. https://doi.org/10.1515/quageo-2017-0007.
Porter, C., Morin, P., Howat, I., Noh, M.J., Bates, B., Peterman, K., Keesey, S., Schlenk, M., Gardiner, J., Tomko, K., Willis, M., Kelleher, C., Cloutier, M., Husby, E., Foga, S., Nakamura, H., Platson, M., Wethington, M., Williamson, C., Bauer, G., Enos, J., Arnold, G., Kramer, W., Becker, P., Doshi, A., D'Souza, C., Cummens, P., Laurier, F., Bojesen, M., 2018. ArcticDEM. In: Harvard Dataverse, 1, pp. 2018–2030.
Prokopiev, A.V., Fridovsky, V.Y., Deikunenko, A.V., 2001. Some aspects of the tectonics of the Verkhoyansk fold-and-thrust belt (northeast Asia) and the structural setting of the Dyandi gold ore cluster. Polarforschung 69, 169–176.
Psomiadis, E., Charizopoulos, N., Soulis, K., Efthimiou, N., 2020. Investigating the correlation of tectonic and morphometric characteristics with the hydrological response in a Greek River catchment using earth observation and geospatial analysis techniques. Geosciences 10 (9), 377. https://doi.org/10.3390/GEOSCIENCES10090377.
Puminov, A.P., 1960. On the history of the river valleys of the lower sections of the Lena and Olenek Rivers. Works of the Research Intitue of Arctic Geology 114 (14), 163–172 (in Russian).
R Core Team, 2021. R: A Language and Environment for Statistical Computing. R Foundation for Statistical Computing, Vienna, Austria. Retrieved March 2024, from. https://www.R-project.org/.
RockWare. RockWorks17 [Software] (n.d.). Retrieved March 2024, from. https://www.rockware.com.
Roy, S.G., Tucker, G.E., Koons, P.O., Smith, S.M., Upton, P., 2016. A fault runs through it: modeling the influence of rock strength and grain-size distribution in a fault-damaged landscape. J. Geophys. Res. Earth 121 (10), 1911–1930. https://doi.org/10.1002/2015JF003662.
Scheiber, T., Fredin, O., Viola, G., Jarna, A., Gasser, D., Łapińska-Viola, R., 2015. Manual extraction of bedrock lineaments from high-resolution LiDAR data: methodological bias and human perception. Gff 137 (4), 362–372. https://doi.org/10.1080/11035897.2015.1085434.
Schirrmeister, L., Wetterich, S., Schwamborn, G., Matthes, H., Grosse, G., Klimova, I., Kunitsky, V.V., Siegert, C., 2022. Heavy and light mineral association of late quaternary permafrost deposits in northeastern Siberia. Front. Earth Sci. 10, 741932 https://doi.org/10.3389/feart.2022.741932.
Schumm, S.A., 1956. Evolution of drainage systems and slopes in badlands at Perth Amboy, New Jersey. Geol. Soc. Am. Bull. 67 (5), 597–646. https://doi.org/10.1130/0016-7606(1956)67[597:EODSAS]2.0.CO;2.
Sekretov, S.B., 2002. Structure and tectonic evolution of the southern Eurasia Basin, Arctic Ocean. Tectonophysics 351 (3), 193–243. https://doi.org/10.1016/S0040-1951(01)00278-5.
Siddiqui, S., Soldati, M., 2014. Appraisal of active tectonics using DEM-based hypsometric integral and trend surface analysis in Emilia-Romagna Apennines, northern Italy. Turk. J. Earth Sci. 23 (3), 277–292. https://doi.org/10.3906/YER-1306-12.
Sim, L.A., Gordeev, N.A., Marinin, A.V., 2018. Modern geodynamics of the eastern boundary of Siberian platform. Geosystems of Transition Zones 2 (4), 280–289 (in Russian).
Skentos, A., 2017. Topographic position index based landform analysis of Messaria (Ikaria Island, Greece). Acta Geobalcanica 4 (1), 7–15. https://doi.org/10.18509/AGB.2018.01.
Stauch, G., Lehmkuhl, F., 2010. Quaternary glaciations in the Verkhoyansk Mountains. Northeast Siberia. Quaternary Research 74 (1), 145–155. https://doi.org/10.1016/j.yqres.2010.04.003.
Strahler, A.N., 1952. Hypsometric (area-altitude) analysis of erosional topography. Geol. Soc. Am. Bull. 63 (11), 1117–1142. https://doi.org/10.1130/0016-7606(1952)63[1117:HAAOET]2.0.CO;2.
Svendsen, J., Alexanderson, H., Astakhov, V.I., Demidov, I., Dowdeswell, J.A., Funder, S., Gataullin, V., Henriksen, M., Hjort, Ch., Houmark-Nielsen, M., Hubberten, H.-W., Ingólfsson, Ó., Jakobsson, M., Kjær, K.H., Larsen, E., Lokrantz, H., Lunkka, J.P., Lyså, A., Mangerud, J., Matiouchkov, A., Murray, A., Möller, P., Niessen, F., Nikolskaya, O., Polyak, L., Saarnisto, M., Siegert, C., Siegert, M.J., Spielhagen, R.F., Stein, R., 2004. Late Quaternary ice sheet history of northern Eurasia. Quaternary Science Reviews 23 (11–13), 1229–1271. https://doi.org/10.1016/j.quascirev.2003.12.008.
Upton, P., Koons, P.O., Roy, S.G., 2018. Rock failure and erosion of a fault damage zone as a function of rock properties: Alpine Fault at Waikukupa River. N. Z. J. Geol. Geophys. 61 (3), 367–375. https://doi.org/10.1080/00288306.2018.1430592.
Vermilye, J.M., Scholz, C.H., 1998. The process zone: a microstructural view of fault growth. J. Geophys. Res. Solid Earth 103 (B6), 12223–12237. https://doi.org/10.1029/98JB00957.
Walbridge, S., Slocum, N., Pobuda, M., Wright, D.J., 2018. Unified geomorphological analysis workflows with Benthic Terrain Modeler. Geosciences 8 (3), 94. https://doi.org/10.3390/geosciences8030094.
Weiss, A., 2001. Topographic position and landforms analysis [Poster presentation]. In: ESRI User Conference 2001, San Diego, CA.
Willgoose, G., Hancock, G., 1998. Revisiting the hypsometric curve as an indicator of form and process in transport-limited catchment. Earth Surface Processes and Landforms: The Journal of the British Geomorphological Group 23 (7), 611–623. https://doi.org/10.1002/(SICI)1096-9837(199807)23:7<611::AID-ESP872>3.0.CO;2-Y.
Wright, D.J., Pendleton, M., Boulware, J., Walbridge, S., Gerlt, B., Eslinger, D., Sampson, D., Huntley, E., 2012. ArcGIS Benthic Terrain Modeler (BTM). v. 3.0.. Environmental Systems Research Institute, NOAA Coastal Services Center, Massachusetts Office of Coastal Zone Management. Retrieved March 2024, from. http://esriurl.com/5754.
Zink, M., Bachmann, M., Brautigam, B., Fritz, T., Hajnsek, I., Moreira, A., Wessel, B., Krieger, G., 2014. TanDEM-X: the new global DEM takes shape. IEEE Geoscience and Remote Sensing Magazine 2 (2), 8–23. https://doi.org/10.1109/MGRS.2014.2318895.